Cellulose (2021) 28:2779–2789
https://doi.org/10.1007/s10570-021-03711-2

ORIGINAL RESEARCH

The colloidal structure of a cellulose fiber

Marta Gubitosi · Shirin Asaadi · Herbert Sixta · Ulf Olsson

Received: 12 February 2020 / Accepted: 21 January 2021 / Published online: 8 February 2021

Abstract We present a small angle X-ray scattering (SAXS) study of the colloidal structure of regenerated cellulose fibers, air-gap spun from an ionic liquid solution. Based on the data, and a different interpretation of the anisotropic SAXS pattern, we propose a slightly different colloidal structure of the fibers, than what is commonly assumed for regenerated cellulose fibers. Fibers with two different degrees of orientation, as produced by different draw ratios, DR = 2 and 15, respectively, are analyzed. The 2D SAXS pattern is highly anisotropic with striking cross-like pattern, having scattering predominantly perpendicular and parallel to the fiber axis. This cross-like pattern suggest a colloidal structure with oriented crystalline lamellae of ca. 10 nm thickness, embedded within a continuous matrix of amorphous cellulose. The lamellae are oriented with their normal parallel with the fiber axis. Complementary wide angle X-ray diffraction data confirm that the lamellae normal direction corresponds to the cellulose chain direction (c-direction) in the monoclinic cellulose crystal (Cellulose II).

Supplementary Information The online version contains supplementary material available at (https://doi.org/10.1007/s10570-021-03711-2).

M. Gubitosi · S. Asaadi · U. Olsson (✉)
Physical Chemistry, Lund University, P. O. Box 124, 221 00 Lund, Sweden
e-mail: Ulf.Olsson@fkem1.lu.se

S. Asaadi · H. Sixta
Department of Forest Products Technology, School of Chemical Technology, Aalto University, P. O. Box 16300, 00076 Aalto, Finland

Graphic abstract

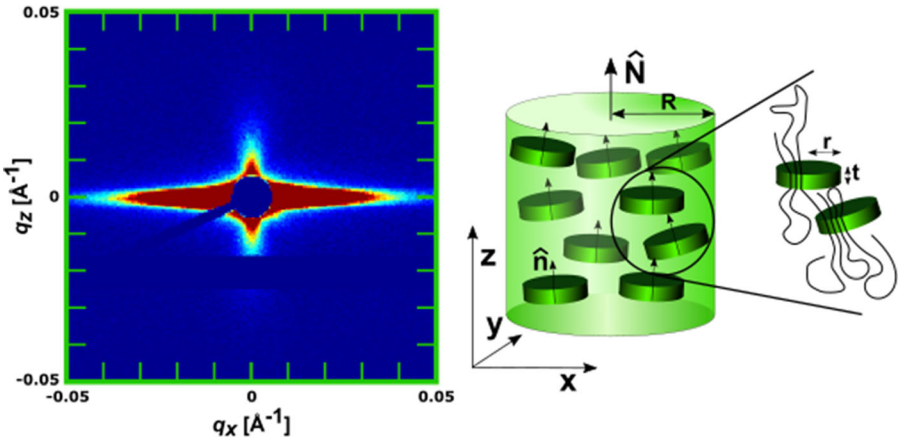

Keywords Regenerated cellulose fibers · SAXS/WAXS · Crystal shape · Crystal orientation

Introduction

Cellulose is the most abundant biopolymer on Earth, and hence an important and renewable raw material. Regenerated cellulose continues to receive increasing attention, as the overall awareness of the need to replace both cotton and petroleum based materials with more environmentally friendly alternatives (Qi 2017; Wang et al. 2016). Textile fibers represent one very important application of regenerated cellulose (Woodings 2001, 1995; Sixta et al. 2015), where the challenge lies in developing new cost efficient, sustainable and environment friendly alternatives to cotton and polyesters.

Regenerated cellulose fibers are spun from solutions, that are extruded, drawn, and then coagulated in an anti-solvent. This coagulation typically involves cellulose crystallization. Polymer crystallization is in fact a complicated molecular process (Keller 1968; Muthukumar 2007), and the effectively final steady state fiber microstructure is not an equilibrium property, but depends e.g. on the dissolution state of cellulose and on process details. As the microstructure in turn dictates the fibers' material properties, it is desired to have a good characterization of the fiber microstructure and knowledge of how it can be tuned by choosing properly the process parameters.

Combined small and wide angle X-ray scattering, SAXS/WAXS, is a useful technique for studying crystalline colloids and semi crystalline materials (Glatter and Kratky 1982; Borsali and Pecora 2008). While SAXS probes the colloidal structure, typically on the 1–100 nm length scale, WAXS gives structural information on the shorter subnanometer length scale where e.g. crystal structure and crystal orientation can be obtained. From extensive SAXS and WAXS studies over the years (French and Langan 2014; Langan et al. 2001; Statton 1956; Schurz and Lenz 1994; Northolt et al. 2001; Crawshaw and Cameron 2000; Vickers et al. 2001; Jiang et al 2012; Chen et al. 2007), the following (generally accepted) picture of the regenerated cellulose fiber structure has emerged. (i) The fibers are semi-crystalline, consisting of both crystalline and amorphous domains, as is typical for crystalline polymers (De Rosa and Auriemma 2014). The crystalline allomorph is the so-called cellulose II, having a monoclinic lattice (Langan et al. 2001). (ii) Due to the extrusion and drawing in the spinning process, the crystalline domains are typically oriented with the chain direction, corresponding to the [00 l] crystal direction, parallel to the fiber axis. Here we have adopted the same convention as in e.g. (Langan et al. 2001), that the cellulose chain direction corresponds to the crystalline *c*-axis and that the length of the *a*-axis is smaller than the *b*-axis. See also French (2014). The degree of orientation depends on the details of the processing. (iii) The fibers are hierarchically made up of elementary fibrils having alternating crystalline and amorphous domains (Schurz

and Lenz 1994; Crawshaw and Cameron 2000). (iv) The crystallites are more extended in the direction of the cellulose chains compared to the perpendicular directions. (v) Dry fibers contain cylindrical voids, typically oriented parallel to the fiber direction. These voids are responsible for the often observed equatorial small angle scattering (Statton 1956; Jiang et al. 2012; Chen et al. 2007).

In the present paper we challenge some of these conclusions and propose a new interpretation of SAXS data, and a new model for the structure of a regenerated cellulose fiber. We present a SAXS and WAXS study of regenerated cellulose fibers, Ioncell-F (Sixta et al. 2015; Asaadi et al. 2018), air-gap spun from an ionic liquid solvent. The structure and the mechanical properties of these fibers were recently characterized (Asaadi et al. 2018). Here we revisit the question of the colloidal structure of regenerated cellulose fibers, basing our discussion on a detailed quantitative analysis of the anisotropic scattering data.

Experimental section

Materials and methods

Enocell birch pre-hydrolyzed kraft pulp (of intrinsic viscosity $[\eta] = 476$ cm^3 g^{-1}, $M_w = 274.3$ kg/mol, Mn = 68.2 kg/mol, polydispersity index PDI = 4) from Stora Enso, Finland was used as a cellulose solute. 1,5-Diazabicyclo[4.3.0]non-5-enium acetate, [DBNH]OAc, ionic liquid was synthesized at Aalto University laboratory and used as solvent. A cellulose solution of 13 wt.% was used for the spinning. The dissolved pulp was spun by dry jet wet spinning. For more details of the spinning process see Asaadi et al. (2018). In short, the cellulose solution was extruded into a water bath through a 36-hole spineret, each hole with a capillary diameter of 100 μm, through an air gap of 10 mm in length. Fibres with two different tensile draw ratios (DR), 2 and 15 were spun, collected, washed and dried.

SAXS measurements and data reduction

All measurements were performed on the Ganesha SAXSlab instrument from JJ X-ray. The instrument had a 300 k Pilatus detector and a Genix 3D X-Ray Source. The X-ray wavelength λ was 1.54 Å. Bundles of parallel fibers (of ca. 50 fibers each) were mounted on the holder using tape, and the holder was inserted in the vacuum chamber. Acquisition times were of 3600 s for all the samples for the q-range $0.06 < q < 1.8$ nm^{-1}, ($q = 4\pi \sin(\theta/2)/\lambda$ where θ is the scattering angle). Dark current subtraction and azimuthal integration were performed using the software Saxsgui (Saxsgui v2.13.02, Rigaku Innovative Technologies, Inc., and JJ X-ray System Aps). The patterns were integrated in an angle range of 20 (or 2) degrees over the meridional and equatorial directions.

Results and discussion

In Fig. 1 we compare the two dimensional scattering patterns, both SAXS and WAXS, from fibers prepared with draw ratios DR = 2 and DR = 15, respectively, where the draw ratio is the ratio between the rate of fiber collection and the rate of extrusion. The vertical orientation of the fibers, and definition of the laboratory frame is illustrated on the right-hand side of Fig. 1. Starting with the WAXS data, we see sharp diffraction spots in the case of DR = 15, demonstrating the presence of crystalline domains that are highly orientationally ordered. For DR = 2 the diffraction peaks show a higher azimuthal broadening compared to DR = 15. The diffraction pattern can be indexed to Cellulose II (Langan et al. 2001), with the crystal c-direction, corresponding to the cellulose chain direction, parallel with the fiber axis.

Also the SAXS data show a significant anisotropy, in particular for DR = 15, with scattering predominantly in the parallel and perpendicular directions to the fiber axis. The small angle scattering from cellulose fibers is often assumed to arise from voids inside the fibers. Here, we argue that the data rather suggest a different origin. The highly anisotropic pattern is likely a superposition of scattering from (at least) two different "objects". The equatorial scattering is associated with objects that have a finite size in the perpendicular direction, but are much larger than $1/q_{min} = 14$ nm in the fiber direction. $q_{min} = 0.07$ nm^{-1} is the lower end of the experimental q-range. The meridional scattering, on the other hand, results from electron density variations in direction of the fiber axis and hence must be associated with the internal structure of the fibers. The highly oriented scattering suggests that it results from domains that

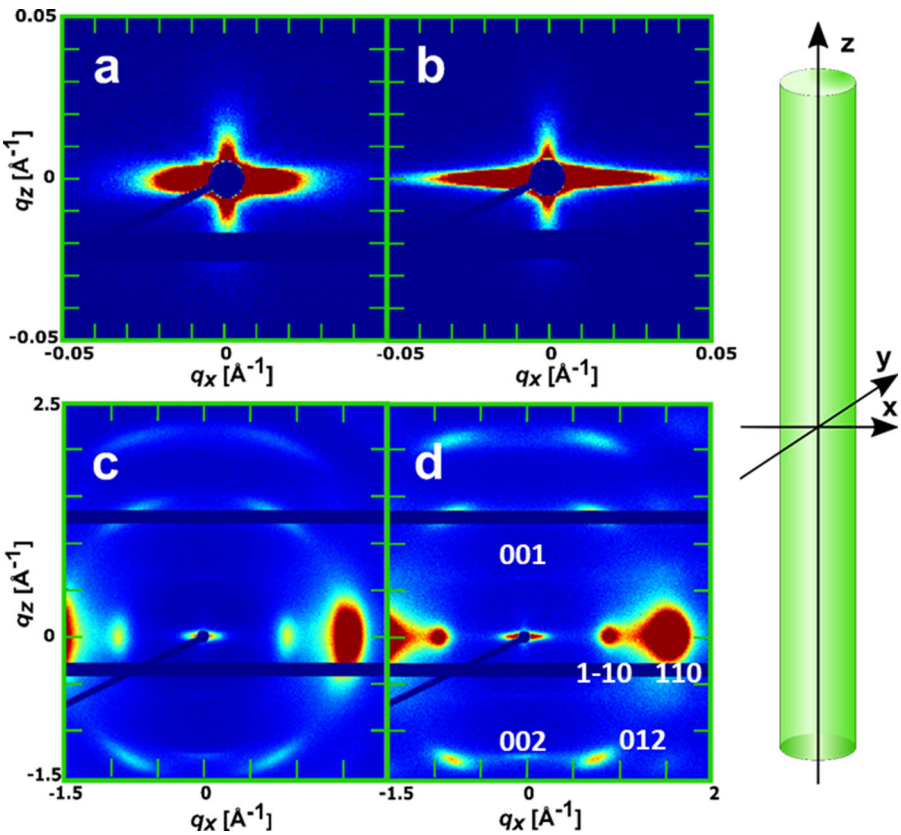

Fig. 1 2D SAXS and WAXS patterns obtained for two different draw ratios. **a** SAXS for DR = 2. **b** SAXS for DR = 15. **c** WAXS for DR = 2. **d** WAXS for DR = 15 together with an assignment, Miller indices (h,k,l), of some of the reflections. To the right is shown an illustration of the fiber orientation and the laboratory coordinate system. Here, z is the meridional direction and the equatorial scattering is recorded in the x-direction

have a finite size in the fiber direction while being large, $> > 1/q_{min}$, in the perpendicular direction.

The degree of crystal orientation can be obtained from an azimuthal plot of a suitable Bragg peak intensity. In Fig. 2 we show such plots, from $\chi = 0°$ to 360°, for DR = 2 and 15, respectively, in the q-band 0.80 $Å^{-1} < q < 0.95$ $Å^{-1}$.χ is the azimuthal angle. The peaks at 0 and 180° appear to be superposition of a narrow and broad component. The narrow component is clearly from the highly ordered crystalline domains. The broad component, we interpret as coming from the amorphous parts of the fibers. To analyze this quantitatively, a model function, consisting of a sum of two Gaussian functions,

$$I(\chi) = A\left(A_c e^{-(\chi-\chi_0)^2/2\sigma_c^2} + A_a e^{-(\chi-\chi_0)^2/2\sigma_a^2}\right) + B \quad (1)$$

centered at $\chi_0 = 0$ and 180°, was calculated and compared to the data. Here, index $i = c$ and a refer to crystal and amorphous domains, respectively, having relative weights A_i and standard deviation σ_i. A is the total amplitude and B is a small background term.

Calculated curves $I(\chi)$ are shown as solid lines. As can be seen, the azimuthal dependence is well described by the sum of two Gaussians. The values of A_i and σ_i are presented in Table 1. The degree of orientation is higher, for the higher draw ratio, as expected. This holds both for the crystalline and the amorphous domains.

The degree of crystal orientation is often quantified in terms of a second rank (Legendre polynomial) order parameter, sometimes referred to as Hermans' orientation parameter

$$P_2 = \frac{1}{2}3\cos^2\vartheta - 1 \quad (2)$$

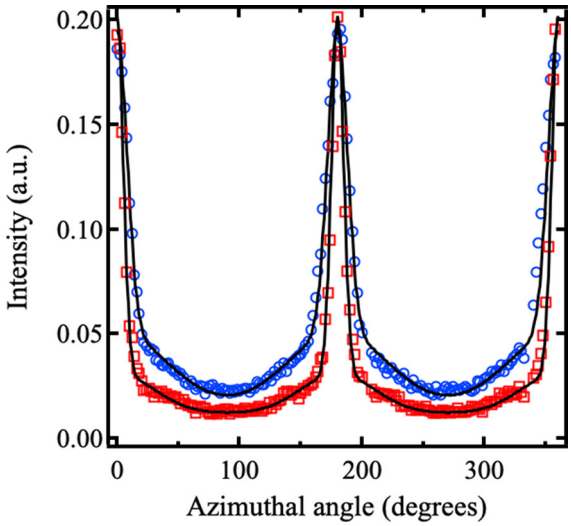

Fig. 2 Azimuthal plots of the intensity in the q-band 0.80 Å^{-1} < q < 0.95 Å^{-1}. Open blue circles are data from DR = 2, while open red squares correspond to DR = 15. The solid lines are calculated curves according to Eq. (1). Parameter values are presented in Table 1

For the crystalline domains, ϑ is the angle between the crystal lamellae normal and the fiber axis. For the amorphous domains, we can identify ϑ as the angle between the local chain orientation and the fiber axis. $< >$ refers to an ensemble average. We can calculate P_2 from the Gaussian distribution functions according to

$$P_2 = \frac{3}{2}\frac{\int d\vartheta exp\{\vartheta/2\sigma^2\} sin\vartheta cos^2\vartheta}{\int d\vartheta exp\{\vartheta/2\sigma^2\} sin\vartheta} - \frac{1}{2} \quad (3)$$

Calculated order parameters for the crystalline and amorphous domains, respectively, are presented in Table 1. The crystalline order parameters, P_{2c}, derived for both samples, are close to unity, which essentially can be inferred directly from the 2D diffraction patters, showing sharp diffraction spots. Also the amorphous domains show a significant degree of chain orientation, with P_{2a} = 0.26 and 0.46 for DR = 2 and 15, respectively. The P_{2c} values reported here are much higher than what has been reported previously for the same fibers (Asaadi et al. 2018). However, the values in that paper were obtained from direct integration of the azimuthal traces and thus contain contributions from both crystal and amorphous domains. Also, a different q-range, 1.3–1.6 Å^{-1}, was used and the background, although small, was not taken into account. The approach used here, should more accurately account for the different contributions.

Table 1 Degree of orientation of crystalline and amorphous domains

Draw ratio	σ_c [a]	P_{2c} [b]	σ_a [c]	P_{2a} [d]	A_c [e]	A_a [f]
DR = 2	8°	0.94	40°	0.26	0.8	0.2
DR = 15	5°	0.98	30°	0.46	0.9	0.1

[a]Standard deviation of crystal orientation distribution as defined in Eq. (1) in degrees

[b]Order parameter for crystal orientation, as defined by Eq. (2)

[c]Standard deviation of cellulose chain orientation distribution in the amorphous domains, as defined in Eq. (1) in degrees

[d]Order parameter for cellulose chain orientation in the amorphous domains orientation, as defined by Eq. (1)

[e]Relative weight of crystal diffraction, as defined by Eq. (1)

[f]Relative weight of amorphous domain scattering, as defined by Eq. (1)

The average orientational chain order parameter (total orientation), $<S>$, was measured by birefringence in Asaadi et al. (2018). For DR = 2 $<S>$ = 0.66 was obtained while for DR = 15, $< S >$ = 0.70. Assuming that $S = \phi_c P_{2c} + (1 - \phi_c)P_{2a}$, where ϕ_c is the volume fraction of crystalline domains, we obtain ϕ_c = 0.59 at DR = 2 and ϕ_c = 0.46 at DR = 15.

In Fig. 3 we have plotted the SAXS data from the meridional, $I(q_z)$, and equatorial, $I(q_x)$, directions respectively. Data from DR = 2 are shown in Fig. 3a, while data from DR = 15 are presented in Fig. 3b. As can be seen, the scattering patterns are significantly different in the two directions. The intensity is higher in the equatorial direction, and also the shapes of the scattering curves are different. On the other hand, the scattering profiles for DR = 2 and DR = 15 are qualitatively similar.

The equatorial scattering shows a q^{-4} power law over a major part of the q-range, leveling off to a constant at high q. The q^{-4} decay can be interpreted as the final slope in a Porod regime (Porod 1982). As we observe this Porod regime all the way down to the lowest q-value, q_{min} = 0.07 nm^{-1}, without reaching a Guinier regime, we may conclude that the objects responsible for the observed scattering have a dimension in the perpendicular direction that is larger than 100 nm.

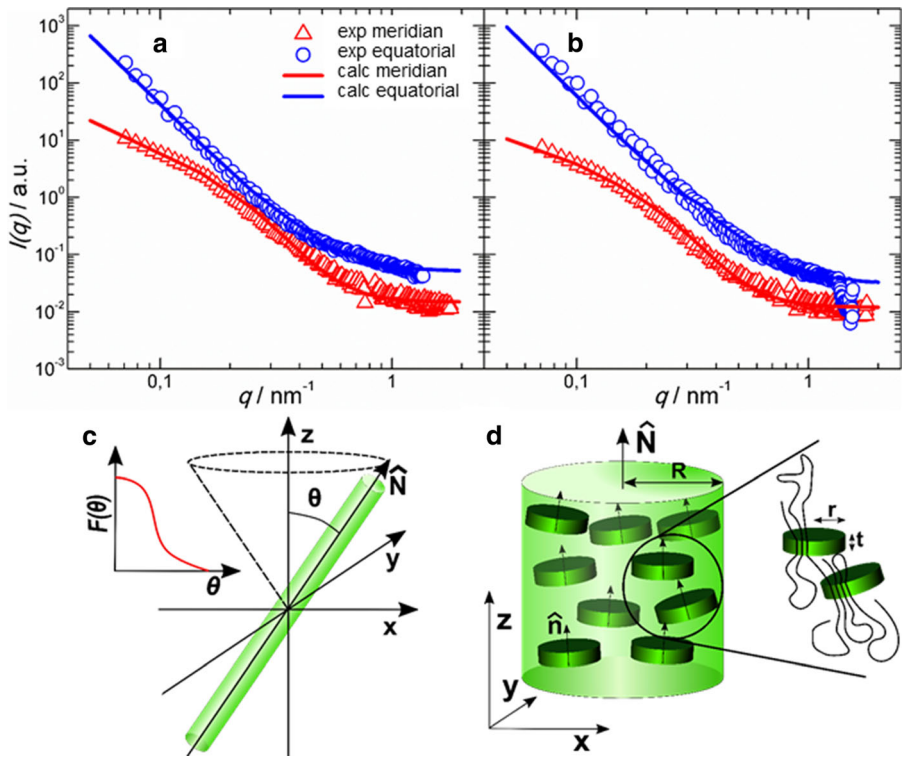

Fig. 3 **a** SAXS patterns recorded along the equatorial (blue circles) and meridional direction (red triangles) for DR = 2. The solid lines are model calculations (see text). **b** Same as in **a** but for DR = 15. **c** Illustration of the fiber orientation distribution with respect to the laboratory frame. We assume a Gaussian distribution of the azimuthal angle, θ, between the fiber normal $\hat{\boldsymbol{N}}$ and the laboratory z-axis, while there is a completely homogeneous distribution in the polar angle. **d** A schematic illustration of the proposed fiber structure. Crystalline lamellae, for simplicity described as circular discs of radius r and thickness t. The lamellae are embedded in an amorphous matrix and are highly oriented. Their layer normal $\hat{\boldsymbol{n}}$ is on the average parallel with the fiber axis $\hat{\boldsymbol{N}}$, with a Gaussian distribution in the azimuthal angle

The small angle scattering from cellulose fiber is often considered to result from voids in the fiber matrix (Statton 1956; Jiang et al. 2012; Chen et al. 2007). In particular in the case of an anisotropic pattern, with a predominant equatorial scattering, this has been suggested to arise from needle-like voids oriented parallel with the fiber axis. As discussed above, the cylindrical objects oriented parallel to the fiber axis, that give rise to the equatorial scattering must have a radius that is significantly larger than 100 nm. Now, since the DR = 15 fiber radius is ca. 6 µm (Asaadi et al. 2018), it seems more reasonable that the equatorial SAXS pattern is the scattering from the overall fibers themselves. The q^{-4} decay also implies that the fiber interface is sharp (on the length scale of q^{-1}).

The meridional scattering looks both qualitatively and quantitatively different. The intensity is lower compared to the equatorial scattering, and decays rather as q^{-2} at lower q-values. Above $q \approx 0.2$ nm^{-1} there is a crossover to a steeper, q^{-4} decay. The highly directional scattering, resulting from highly directional electron density variations, suggests the presence of domains or particles that have a relatively small dimension in the fiber direction and much larger dimensions ($>> 1/q_{min}$) in the plane perpendicular to that. As will be discussed in further detail below, we propose that this scattering is associated with disc-like crystalline lamellae embedded in a continuous matrix of amorphous cellulose, as schematically illustrated in Fig. 3d. Polymers are in fact known to crystalize in a lamellar structure with a 10–20 nm thickness (Keller 1979; Welch and Muthukumar 2001; Wang 2007), and it is therefore reasonable to assume that the lamellar particles giving rise to the meridional scattering indeed are the crystallites. That the amorphous part

forms a continuous matrix seems also to be consistent with water swelling experiments (Asaadi et al. 2018). Immersing the fibers in water resulted in a homogeneous swelling of the fiber radius. We expect mainly the amorphous domains to swell. If the crystalline part would be continuous, with amorphous inclusions, we would not have expected any significant swelling.

For a more quantitative analysis, we consider the form factors of the fibers and the crystallites. We can derive model scattering functions in the two directions on the same relative intensity scale so that they can be compared and analyzed together. Using the equatorial fiber scattering intensity as a reference, we can evaluate the parallel scattering more quantitatively. The fibers we model as homogeneous cylinders of scattering length density ρ. For a given orientation, the form factor is given by (Pedersen 1997)

$$P_f(q) = \left[\frac{2J_1(q\,R\,sin\alpha)}{q\,R\,sin\alpha}\frac{\sin(\,qL\,cos\alpha/2)}{q\,L\,cos\alpha/2}\right]^2 \tag{4}$$

where $J_1(x)$ is the first order Bessel function, L is the length, R the radius of the cylinder and α is the angle between the cylinder axis and the q-vector. In the experiments, the fibers have been oriented vertically, *i.e.* parallel to the z-axis. However, there is a distribution of orientations that, although being narrow, influences the scattering and needs to be taken into account. The orientation of the fiber axis $\hat{\boldsymbol{N}}$ can be described by the polar angle θ, *i.e.* the angle between $\hat{\boldsymbol{N}}$ and the z-axis, and the azimuthal angle, φ, in the xy plane. We assume here a homogeneous distribution of φ and a narrow Gaussian distribution of θ, $f_f(\theta) = exp\{-\theta^2/2\sigma_\theta^2\}$, with a standard deviation σ_θ. In the equatorial direction, the total scattered intensity can then be defined as

$$I(q_x) = \frac{N_f\rho^2}{\int f_R(R)\left(\iint f_f(\theta)d\theta d\varphi\right)dR}\int f_R(R)V_f^2 \left(\iint f_f(\theta)P_f(R,q_x)d\theta d\varphi\right)dR \tag{5}$$

where N_f is the number of fibers and $V_f = \pi R^2 L$ is the fiber volume. While N_f enters as a trivial proportionality constant in both $I(q_x)$ and $I(q_z)$, and could have been ignored, we still keep it in the equations as a formality. In fact, one may consider an experiment where N_f is controlled and the intensity is recorded on an absolute scale. The fiber length, L, here we have set to the length exposed to the X-ray beam and hence corresponds to the effective beam dimension in the z-direction. In the calculations we have fixed L to 0.25 mm. We also take into account a polydispersity in the fiber radius, assuming a Gaussian distribution, $f_R(R) = exp\left\{-(R-R)^2/2\sigma_R^2\right\}$, around the average value $<R>$, with a standard deviation σ_R.

The internal fiber structure we model as crystalline discs embedded in a continuous amorphous matrix. For the crystalline discs we use the same cylinder form factor (Eq. (4)), although now $L << R$. We change the notation, however, and, instead of L, denote the disc thickness t, and the disc radius r. Thus, we write

$$P_c(q) = \left[\frac{2J_1(q\,r\,sin\alpha)}{q\,r\,sin\alpha}\frac{\sin(q\,t\,cos\alpha/2)}{q\,t\,cos\alpha/2}\right]^2 \tag{6}$$

for the crystallite form factor. As for the fiber radius above, we also include a polydispersity in the thickness, t, assuming a Gaussian distribution, $f_t(t) = exp\left\{-(t-t)^2/2\sigma_t^2\right\}$, around the average value $< t >$, with a standard deviation σ_t. While the disc radius is most likely also polydisperse, we can neglect this here as the sizes seem to be larger than $1/q_{min}$. The crystalline discs are highly oriented in the fibers with their normal, $\hat{\boldsymbol{n}}$, essentially parallel to the fiber axis, $\hat{\boldsymbol{N}}$, although with some distribution in orientation. We take this distribution into account by again assuming a homogeneous distribution with respect to the azimuthal angle, here denoted ψ, and a Gaussian distribution of the polar angle, ϑ (the angle between $\hat{\boldsymbol{n}}$ and $\hat{\boldsymbol{N}}$), $f_c(\vartheta) = exp\{-\vartheta^2/2\sigma_\vartheta^2\}$ with a standard deviation σ_c. In the calculation of $I(q_z)$ we thus need in principle to average over 4 angles, two describing the fiber orientation with respect to the laboratory frame, and two describing the crystallite orientation with respect to the fiber axis. However, since the distribution in fiber orientation can essentially be neglected, $\sigma_\vartheta \gg \sigma_\theta \approx 0$, we have in the numerical calculations assumed $\sigma_\theta = 0$. In this case we can write

$$I(q_z) = \frac{\phi_c\Delta\rho^2 N_f}{\int f_R(R)\left(\int f_t(t)\left(\iint d\vartheta d\psi f_c(\vartheta)\right)dt\right)dR}\int f_R(R)V_f \left(\int f_t(t)V_c\left(\iint f_c(\vartheta)P_c(t,q_z)d\vartheta d\psi\right)dt\right)dR \tag{7}$$

Table 2 Parameter values in model calculations of $I(q_x)$ and $I(q_z)$

	L/mm[a]	$< R >$/μm[b]	σ_R/μm	$< t >$/nm	Σ_t/nm	r/nm	ρ/cm^{-2}	$\Delta\rho$/cm^{-2} [c]	σ_θ	σ_ϑ [d]	ϕ_c
DR = 2	0.25	16	3.2	10	4.5	300	1.35×10^{11}	$1.2\ 10^{10}$	0.1°	8°	0.15
DR = 15	0.25	5.6	1.1	10	4.5	300	$1.35 \times w10^{11}$	$1.2\ 10^{10}$	0.1°	5°	0.28

[a]Estimated from the primary beam diameter. This parameter scales the intensity equally in the meridional and equatorial directions

[b]Average value measured in Asaadi et al. (2018)

[c]Assuming that the amorphous domains have a mass density that is 91% of that of crystalline domains (Fink and Walenta 1994)

[d]Values taken from Table 1

Here, ϕ_c is the volume fraction of crystalline domains within the fiber, $V_c = \pi r^2 t$ is the crystallite volume, and $\Delta\rho$ is the scattering length difference between the crystalline and amorphous domains.

In the numerical model calculations of $I(q_x)$ and $I(q_z)$, the polydispersity in R and t were taken into account by summing over 11 different values homogeneously distributed in the range from -2 to 2 standard deviations, each with the correct weight. In order to account for the orientational distribution, for each value of R and t, there was also a weighted summation over 40 different values of θ and ϑ, respectively, equally spaced in the range from 0 to 2 standard deviations. Finally, for each value of θ and ϑ, there was a summation over 100 distributed values of the azimuthal angle, equally spaced in the range from 0 to 2π, and all having the same weight.

Calculated scattered intensities are shown as solid lines in Fig. 3a, b, with parameter values summarized in Table 2. For the crystallite-amorphous contrast we have assumed that the amorphous part has a mass density being 91% of the crystalline density (Fink and Walenta 1994). The average fiber radius, $< R >$, has been determined previously (Asaadi et al. 2018) and σ_υ is fixed from the azimuthal analysis (Table 1). $L = 0.25$ mm was the estimated beam diameter, and was not varied. $r = 300$ nm was chosen mainly as a size $> 1/q_{min}$, and was also not varied.

This quantitative analysis of SAXS data is based on the assumption that the equatorial small angle scattering corresponds the overall Porod (interfacial) scattering from the fibers, allowing us to use this as a kind of internal calibration of the scattered intensity. While the analysis performed involves a large number of parameters, several of them are fixed in the calculations. The adjustable parameters were the polydispersity parameters σ_R and σ_t, the (low) standard deviation of fiber orientation distribution that we fix to $\sigma_\theta = 0.1°$, the lamellae thickness, t, and the crystal volume fraction, ϕ_c. We note that the model scattering curves in Fig. 3a, b are calculations and not least squares fits. It is difficult to determine the uncertainty in the different parameter values. However, we conclude that the parameter values given in Table 2 are all reasonable. As supplementary material we present calculations where we compare model curves with some different values of t and σ_t.

In the analysis above, we have neglected possible contributions to the scattering coming from interparticle correlations, assuming that the meridional structure factor $S(q_z) \approx 1$. This does not seem consistent with the fact that the crystallinity appears to be high, of the order of 50%. From repulsive excluded volume interactions we would expect a lowering of the intensity at lower q-values, due to $S(0) < 1$, and possibly also a structure factor peak if the stacking of lamellae have a significant periodicity. A well defined stacking periodicity is for example observed when polyethylene is crystallized from o-xylene. (Wang 2007). A meridional peak, although weak, has also been reported for regenerated cellulose fibers (Statton 1956). The fact that we do not observe a meridional correlation peak in the present fibers is somewhat striking, considering also the high degree of orientational order. A high polydispersity in t is expected to make the periodicity less well defined. Another possible explanation could be that the distribution of crystallites is not homogeneous, but rather heterogeneous with domains of low and high concentration respectively also contributing to a wide distribution in interparticle spacing. The uncertainty regarding $S(q_z)$, adds an uncertainty to the deduced parameters in the analysis. In particular to the volume fraction of

crystallites that in the model is proportional to the overall scattered intensity.

The scattering curves in both the equatorial and meridional directions level off to a constant at high q. At these high q-values the scattered intensity now reports on electron density fluctuations and hence the structure on the molecular length scale. We are also approaching the q-regime where we obtain Bragg reflections from the crystalline domain. The constant intensity here is ca. 4 times higher in the equatorial compared to the meridional direction. This difference we can understand from the fact that the cellulose chains are strongly oriented parallel to the fiber axis. For this reason, we expect larger amplitude electron (and mass) density variations perpendicular to the chains, compared to the direction along the chains.

The lamellar thickness, t, can also be estimated from *e.g.* the width of {002} reflection in the q_z direction using the Scherrer equation, that approximately can be written as $t \approx 6/\Delta q$, where Δq is the peak width at half height (Patterson 1939). The {00 k} peaks are very weak, because of the strongly oriented crystallites having <00k> directions parallel with the z-axis. At these wide angles, of the order of 20°, the $\boldsymbol{q}$ vector makes a significant angle ($\approx$ 10°) with the xz plane and there are only a few crystallites that meet the Bragg condition, $\boldsymbol{q}$// <00k> . Nevertheless, when analyzing the width of the {002} reflection in the parallel direction we obtain $t \approx$ 15 nm.

In the equatorial plane, on the other hand, the Bragg condition is well met at many places in the fibers and strong {hk0} reflections are observed. In Fig. 4 we have plotted the wide angle scattered (diffracted) intensity in the perpendicular, x-direction, for several draw ratios. The different diffraction curves have been multiplied with a proportional constant to have the same arbitrary intensity at q_x = 20 nm^{-1}. When doing so, all curves strikingly fall onto one master curve, showing that the peak widths are independent of the draw ratio. For the {1–10} reflection at 8.7 nm^{-1} we estimate $\Delta q \approx 1$ nm^{-1}. Applying the Scherrer equation this corresponds to a crystallite width of 6 nm in the equatorial < 1–10 > direction. The {110} and {200} peaks at 14.1 and 15.6 nm^{-1}, respectively, appear to have similar Δq. A crystallite with of 6 nm is not consistent with our interpretation of the highly directional meridional SAXS pattern above, in terms of disc-like crystallites with diameters of several hundred nm. However, a finite crystallite size is not the only possible source of peak broadening. Another potential source is defects in the crystal packing. Polymer crystals typically involve folded chains (Keller 1968) and a common dislocation defect could be chain folding and chain ends within the crystalline domains. However, considering the highly oriented chains, in combination with that the persistence length of cellulose is of the order of 10 nm (Kroon-Batenburg et al. 1997; Martin-Bertelsen et al. 2020) (same order of magnitude as t), the degree of chain folding may be low. Nevertheless, the 6 nm length scale should in this case be interpreted as a correlation length of the periodic structure within the crystallites. More work is needed in order to unravel the highly constant peak shapes in Fig. 4.

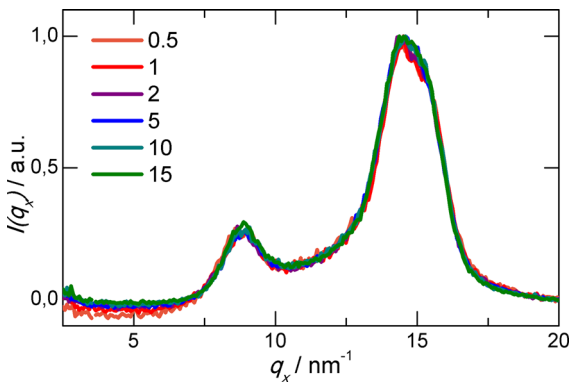

Fig. 4 Diffraction in the perpendicular (equatorial) direction, here denoted x, for different draw ratios DR = 0.5, 1, 2, 5, 10, and 15, respectively

Conclusions

We have analyzed the SAXS and WAXS patterns of a regenerated cellulose fiber, produced with two different draw ratios, DR = 2 and DR = 15, respectively. Highly oriented wide angle diffraction patterns are observed that can be indexed to Cellulose II, and demonstrates that the crystallites are strongly oriented with the c-axis parallel with the fiber axis. The degree of orientation is higher for the larger draw ratio, and was determined for both the crystallites and the chains in the amorphous domains, respectively The most striking observation is the highly anisotropic cross-like SAXS pattern, with scattering essentially exclusively in the perpendicular meridional and equatorial directions, respectively. We conclude that the

equatorial scattering corresponds to the overall fiber scattering in the direction perpendicular to the fiber axis, while the meridional scattering reports on the internal fiber structure. We show that the meridional SAXS pattern is consistent with lamellar particles, having thickness of ca. 10 nm, highly oriented with their normal in the fiber direction. We propose that these lamellae correspond to the crystalline domains, that are embedded in an amorphous non-crystalline continuous matrix. The cellulose chains in the amorphous matrix are also somewhat stretched and have a preferred orientation in the fiber direction. We note that cellulose regeneration is a polymer crystallization process. The fact that polymers in general typically crystallize into lamellae support the proposed structure. As a particular feature of the analysis, the equatorial scattering intensity in the Porod regime was used as a standard to calibrate intensity.

Acknowledgments This work was supported by the Swedish Research Council. The stay of AS in Lund was supported by COST Action STSM FP1205. UO thanks Masayuki Imai, Tohoku University, for stimulating discussions.

Funding Open Access funding provided by Lund University. This work was supported by the Swedish Research Council. The stay of AS in Lund was supported by COST Action STSM FP1205.

Compliance with ethical standards

Conflict of interest The authors declare that they have no conflict of interest.

References

Asaadi S, Hummel M, Ahvenainen P, Gubitosi M, Olsson U, Sixta H (2018) Structural analysis of ioncell-F fibres from birch wood. Carbohydr Polym 181:893–901

Borsali R, Pecora R (eds) (2008) Soft matter characterization. Springer, New York

Chen X, Burger C, Wan F, Zhang J, Rong L, Hsiao BS, Chu B, Cai J, Zhang L (2007) Structure study of cellulose fibers wet-spun from environmentally friendly NaOH/urea aqueous solutions. Biomacromol 8:1918–1926

Crawshaw J, Cameron RE (2000) Small angle X-ray scattering study of pore structure in tencel® cellulose fibres and the effects of physical treatments. Polymer 41:4691–4698

De Rosa C, Auriemma F (2014) Crystals and crystallinity in polymers. Wiley, Hoboken

Fink HP, Walenta E (1994) Röntgenuntersuschungen zur übermolekularen Struktur von Cellulose im Verarbeitungprozess. Das Pap 12:739–748

French AD (2014) Idealized powder diffraction patterns for cellulose polymorphs. Cellulose 21:885–896

French A, Langan P (2014) 100 years of cellulose fiber diffraction and the emergence of complementary techniques. Cellulose 21(3):1087–1089

Glatter O, Kratky O (eds) (1982) Small angle X-ray scattering. Academic Press, London

Jiang G, Huang W, Li L, Wang X, Pang F, Zhang Y, Wang H (2012) Structure and properties of regenerated cellulose fibers from different technology processes. Carbohydr Polym 87:2012–2018

Keller A (1968) Polymer crystals. Rep Prog Phys 31:623–704

Keller A (1979) Crystalline polymers; an introduction. Faraday Discuss Chem Soc 68:145–166

Kroon-Batenburg LMJ, Kruiskamp PH, Vliegenthart JFG, Kroon J (1997) Estimation of the persistence length of polymers by MD simulations on small fragments in solution. Appl Cellulose J Phys Chem B 101:8454–8459

Langan P, Nishiyama Y, Chanzy H (2001) X-ray Structure of mercerized cellulose II at 1 Å resolution. Biomacromol 2:410–416

Martin-Bertelsen B, Andersson E, Köhnke T, Hedlund A, Stigsson L, Olsson U (2020) Revisiting the dissolution of cellulose in NaOH as "seen" by X-rays. Polymers 12:342

Muthukumar M (2007) Shifting paradigms in polymer crystallization. In: Reiter G, Strobl GR (eds) Progress in understanding polymer crystallization. Vol 714. Lecture Notes in Physics. Springer Berlin, pp 1–18

Northolt MG, Boerstoel H, Maatman H, Huisman R, Veuring J, Elzerman H (2001) The structure and properties of cellulose fibres spun from an anisotropic phosphoric acid solution. Polymer 42:8249–8264

Patterson AL (1939) The Scherrer formula for X-ray particle size determination. Phys Rev 56:978–982

Pedersen JS (1997) Analysis of small-angle scattering data from colloids and polymer solutions: modeling and least-squares fitting. Adv Colloid Interface Sci 70:171–210

Porod G (1982) In Glatter O, Kratky O (eds) Small angle X-ray scattering. Academic Press, London, pp 17–51

Qi H (2017) Novel functional materials based on cellulose. Springer briefs in applied sciences and technology. Springer, Berlin

Schurz J, Lenz J (1994) Investigations on the structure of regenerated cellulose fibers. Macromol Symp 83:273–289

Sixta H, Michud A, Hauru L, Asaadi S, Ma Y, King AWT, Kilpäleinen I, Hummel M (2015) Ioncell-F: a high-strength regenerated cellulose fibre. Nord Pulp Pap Res J 30:43–57

Statton WO (1956) Crystallite regularity and void content in celulose fibers as shown by small-angle X-ray scattering. J Polym Sci 22:385–397

Vickers ME, Briggs NP, Ibbet RN, Payne JJ, Smith SB (2001) Small angle X-ray scattering studies on lyocell cellulosic fibres: the effects of drying Re-Wetting and Changing Coagulation. Temp Polym 42:8241–8248

Wang H (2007) Small angle scattering study of polyethylene crystallization from solution. In: Reiter G, Strobl GR (eds) Progress in understanding polymer crystallization, Vol 714. Lecture Notes in Physics. Springer Berlin, pp 169–178

Wang S, Lu A, Zhang L (2016) Recent advances in regenerated cellulose materials. Prog Polym Sci 53:169–206

Welch P, Muthukumar M (2001) Molecular Mechanisms of polymer crystallization from solution. Phys Rev Lett 87:218302–218304

Woodings CR (1995) The development of advanced cellulosic fibres. Int J Biol Macromol 17:305–309

Woodings C (ed) (2001) Regenerated cellulose fibres. Woodhead Publishing Ltd., Cambridge